CrystEngComm

Accepted Manuscript

ROYAL SOCIETY OF CHEMISTRY

www.rsc.org/crystengcomm

Journal Name

ARTICLE

Synthesis of mesporous and tetragonal zirconia with inherited morphology from metal-organic frameworks

Received 00th January 20xx,
Accepted 00th January 20xx

DOI: 10.1039/x0xx00000x

www.rsc.org/

Xiaoliang Yan, Ningyue Lu, Binbin Fan*, Jiehua Bao, Dahai Pan, Meijun Wang and Ruifeng Li*

Controlled synthesis of porous metal oxides with desired morphology has been motivating scientists to explore and develop new preparation methodologies. Among them, thermal decomposition of metal-organic frameworks (MOFs) has been employed for the fabrication of several metal oxides. In this work, this strategy is employed to prepare mesoporous and tetragonal zirconia (t-ZrO_2) from metal-organic framework (UiO-66), acting as both morphological template and zirconium source. This process avoids the use and removal of extra template as well as the addition of stabilizers for t-ZrO_2. After thermal decomposition at 500 °C, t-ZrO_2 inherited octahedral morphology from the pristine precursor, and possessed small nanoparticles with an average size of 3.1 nm. The derived t-ZrO_2 had a large surface area of 174 m^2/g and the pore diameter of 5–8 nm. The formation mechanism of t-ZrO_2 was also discussed. This simple and potentially universal strategy can be used to fabricate porous metal oxides with desired shape for many applications.

Introduction

The design and synthesis of porous metal oxides with unique morphology have been attracting great attention in many research fields. Traditionally, structure-directing agents and/or self-assembly surfactants were used for the synthesis of mesoporous metal oxides, including TiO_2, ZrO_2, Al_2O_3, WO_3, SnO_2, and Fe_2O_3.[1–4] In addition, the hard-templating method was also employed to prepare mesoporous metal oxides.[5–8] For example, porous metal oxides (Al_2O_3, TiO_2, V_2O_5, and ZnO) with different morphologies were synthesized by using carbon nanotubes as templates.[7] In this method, crystallization temperature and the surface coverage of metal oxides along with oxidation temperature of the carbon nanotubes played significant roles in the final morphology of the products.

Recently, metal oxides with different morphologies have been prepared by thermal decomposition of metal-organic frameworks (MOFs), which are consisted of metal ions and organic linkers.[9–14] For example, Co_3O_4 hexagonal nanorings were prepared by calcination of Co-based organic frameworks and organic amine.[9] α-Fe_2O_3 and Fe_3O_4 nanorods were obtained by controlling the calcination conditions of Fe-MIL-88B.[10] Highly dispersed iron carbides in porous carbon matrix were synthesized from Fe-based MOF Basolite F300.[11] Mesoporous Cr_2O_3/Al_2O_3 with large specific surface area and high pore volume was synthesized using MIL-101 as host matrix and chromium precursor along with aluminium isopropoxide as aluminium precursor.[12] Furthermore, there are systematic reviews that demonstrate the use of MOFs for the synthesis of porous metal oxide by thermal decomposition, including Co_3O_4, Fe_2O_3, CuO, γ-MnO_2, ZnO, and In_2O_3.[13,14] More recently, yttria stabilized zirconia (YSZ) was obtained from Y-doped MOFs by two-step thermal treatment in an inert atmosphere and then in oxygen.[15] The derived YSZ had large surface area, crystalline framework, and high oxygen ion conductivity. Also, a new scalable synthesis strategy for the preparation of octahedral Cr_2O_3 with large surface area and porosity was reported by combustion synthesis using MIL-101(Cr) as a sacrificial template.[16] However, the structure and morphology of MOFs of evolutions to the derived sample were not well established. In this work, metal-organic framework (UiO-66), as zirconium-containing precursor and morphological template, was developed to produce ZrO_2 by thermal decomposition in air. The derived ZrO_2 well inherited the pristine morphology of precursor and showed pure tetragonal phase with mesoporous structure and small nanoparticles. The formation mechanism of t-ZrO_2 was demonstrated on the basis of transmission electron microscopy (TEM), scanning electron microscopy (SEM), Raman spectroscopy, X-ray diffraction (XRD), and thermo-gravimetric (TG) analyses.

College of Chemistry and Chemical Engineering, Taiyuan University of Technology, Taiyuan 030024, China
Email: yanxiaoliang@tyut.edu.cn, fanbinbin@tyut.edu.cn, rfli@tyut.edu.cn
Fax: (+86) 351 6010121
Tel: (+86) 351 6018384
† Footnotes relating to the title and/or authors should appear here.
Electronic Supplementary Information (ESI) available: [details of any supplementary information available should be included here]. See DOI: 10.1039/x0xx00000x

Experimental

Synthesis of UiO-66 UiO-66 was prepared and purified according to a previously published procedure.[17] In a typical procedure, a mixture of $ZrCl_4$ (8 mM) and 1, 4-benzene-dicarboxylate (BDC, 8 mM) was dissolved in 10 mL of DMF containing acetic acid (2.4 M). The mixture was placed at 120 °C for 24 h. The reaction product was collected by centrifugation, washed with DMF three times, and soaked in methanol at 60 °C for three days with replacing the soaking solvent every 24 h to exchange DMF. Finally, the product was washed with methanol three times.

Synthesis of t-ZrO_2 For the thermal decomposition process, the as-obtained UiO-66 was calcined at 500 °C in air for 6 h with a heating rate of 10 °/min.

Synthesis of UiO-66-HCl UiO-66-HCl was prepared from a mixture of zirconium tetra-chloride ($ZrCl_4$), terephthalic acid, hydrochloric acid, and dimethyl-formamide in the 25 mmol: 50 mmol: 50 mmol: 150 mL ratio.[18] The slurry was then transferred into a 450 mL Teflon and was heated at 220 °C for 16 h. The resulting white product was filtered, washed with DMF to remove unreacted terephthalic acid, and then washed with acetone and dried at room temperature. The sample was finally calcined at 250 °C under vacuum to remove the DMF from the framework.

Synthesis of t-ZrO_2-HCl The process was the same as the synthesis of t-ZrO_2 except the use of UiO-66-HCl as a precursor.

Characterizations XRD analysis was performed with a Rigaku D/MAX-2500 V/PV diffractometer using Cu-Kα radiation (40 kV and 200 mA) at a scanning speed of 4°/min. Raman spectroscopy was carried out on a Renishaw inVia Raman Microscope using a 532 nm wavelength as the excitation source. TEM observations were carried out using JEM100CXII operated at 100 kV. A small quantity of samples ethanol solution was dropped onto the 300 mesh copper TEM grid. SEM images (powder samples) with energy dispersive X-ray spectra (EDS) were recorded with Hitachi field emission scanning electron microscope (S4800). Physisorption of N_2 was performed at −196°C using a Quantachrome Nova 1200e. Before measurement, the sample was evacuated at 250 °C for 3 h. The surface area was calculated by BET method at relative pressure of P/P_0 = 0.05–0.25. The pore diameter value was calculated by BJH method. TG analysis was carried out using a Netzsch STA 449 F3 system with a heating rate of 10 °C min^{-1} under flowing air (25 mL min^{-1}).

Results and Discussion

Structure and morphology characterizations

Fig. S1 and Fig. 1a show XRD patterns of UiO-66 and the as-obtained sample, respectively. The relative intensity and peak positions of UiO-66 in the XRD pattern are consistent with previous report[17] and the simulated one (Fig. S1), conforming the formation of desirable UiO type crystalline framework. After the treatment of UiO-66 at 500 °C, the Bragg reflections of UiO-66 disappear and new diffraction peaks are clearly observed. Four broad peaks at 30.2°, 34.8°, 50.4°, and 59.6° are characteristic for the presence of tetragonal phase of ZrO_2 (t-ZrO_2). Other types of ZrO_2, e.g. monoclinic and mixed phases, are not detected. The broad XRD diffraction peaks of the derived t-ZrO_2 are due to the small crystallite size (~3.94 nm), as calculated by the Scherrer equation. Since the tetragonal and cubic (c-ZrO_2) phases of ZrO_2 exhibit similar XRD patterns, Raman spectroscopy, which is highly sensitive to the polarizability of the oxygen ions, was used to distinguish between t- and c- ZrO_2. As shown in Fig. 1b, the Raman peaks at 145, 275, 460, and 640 cm^{-1} can be attributed to t-ZrO_2, whereas the peak at 490 cm^{-1} characteristic for c-ZrO_2 is not detected, indicating the transformation of the pristine UiO-66 to the derived t-ZrO_2 by thermal decomposition.

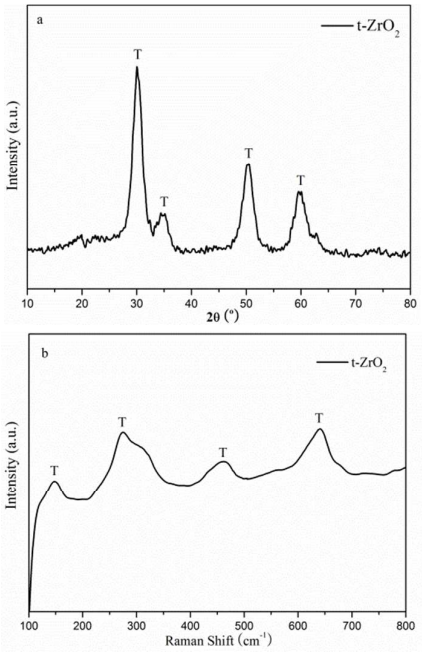

Fig. 1. (a) XRD pattern and (b) Raman spectrum of t-ZrO_2 obtained from thermal decomposition of UiO-66 at 500 °C.

Morphological change of UiO-66 to the derived t-ZrO_2 was illustrated by SEM observations (Fig. S2 and Fig. 2). Mono-dispersed octahedral microcrystals of UiO-66 are shown in Fig. S2. As shown in Fig. 2, the derived t-ZrO_2 has octahedral morphology, which is similar to that of the precursor, indicating the morphological inheritance of product from UiO-66. Interestingly, the most octahedrons of t-ZrO_2 have rough surfaces, which are formed by rod-like zirconia. The cavity of the octahedron of t-ZrO_2 becomes smaller than that of the original UiO-66, because of the decomposition of the organic compounds in the framework. The inheritance of morphology from UiO-66 to product is also clarified by EDS mapping analysis (Fig. 3). The mapping of t-ZrO_2 consists of elements Zr (yellow) and O (red). The Zr and O mappings of t-ZrO_2 satisfy with the octahedral structure. The phenomena that the derived metal oxides inherit the morphology from the MOFs have also been reported in the literatures. For example, mesoporous Al_2O_3 was synthesized by direct thermal

treatment of Al-based MOFs, and the fibrous morphology and hexagonal spindle-shape of original MOFs were well maintained.[19,20]

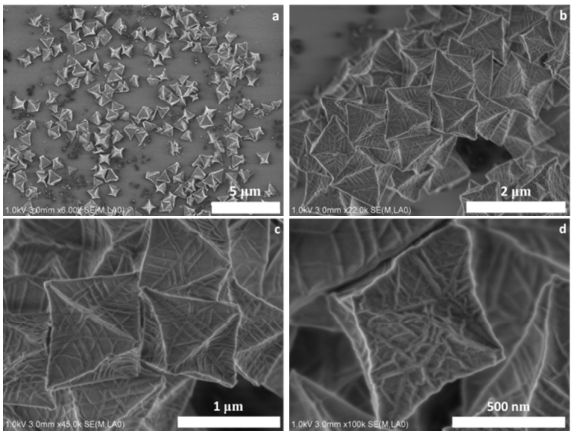

Fig. 2. SEM images of t-ZrO_2.

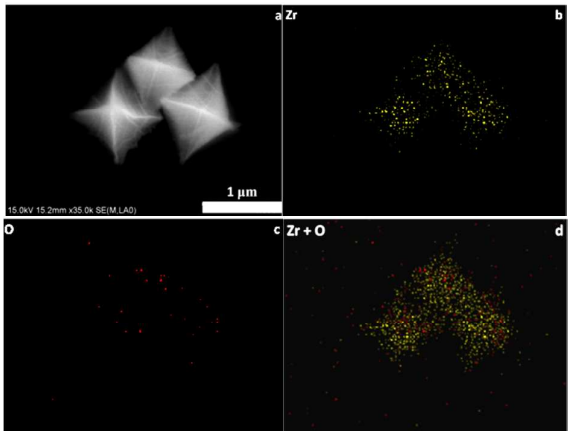

Fig. 3. EDS mapping images of t-ZrO_2.

TEM images of the derived t-ZrO_2 are shown in Fig. S3 and Fig. 4. In a low magnification TEM image (Fig. S3), octahedral t-ZrO_2 is uniformly dispersed on the substrate and the size of each octahedron is ~1 μm. The derived t-ZrO_2 has hollow octahedral structure with smaller cavity in comparison with UiO-66 (Fig. 4a). An enlarged TEM image in Fig. 4b depicts the existence of high dispersed ZrO_2 nanoparticles and the formation of channels between these nanoparticles. Fig. 4c shows the high-resolution TEM image of the nanoparticles, in which the lattice spacing of 0.295 nm corresponds to the (0 1 1) crystal face of t-ZrO_2. SAED analysis of the nanoparticles in Fig. 4d shows a ring-like diffraction pattern with dispersed bright spots, which is attributed to the existence of tetragonal phase of ZrO_2. Generally, it has been reported that thermal treatment is indispensable for the preparation of fully crystalline ZrO_2 nanoparticles.[21] However, thermal treatment makes the particle size control difficult. In this work, the particle size distribution of t-ZrO_2 was studied by surveying 200 particles from the TEM images (Fig. 5). It can be clearly seen that the particle size has a narrow distribution with the average particle size of 3.1 nm, and the particle size is most in the range of 2–5 nm. The discrete Zr-containing clusters in UiO-66 may play an important role on the stabilization of small nanoparticles. The organic species is removed by thermal decomposition at 500 °C in air, leading to the assembly of the zirconia clusters and generation of zirconia nanoparticles from these clusters.

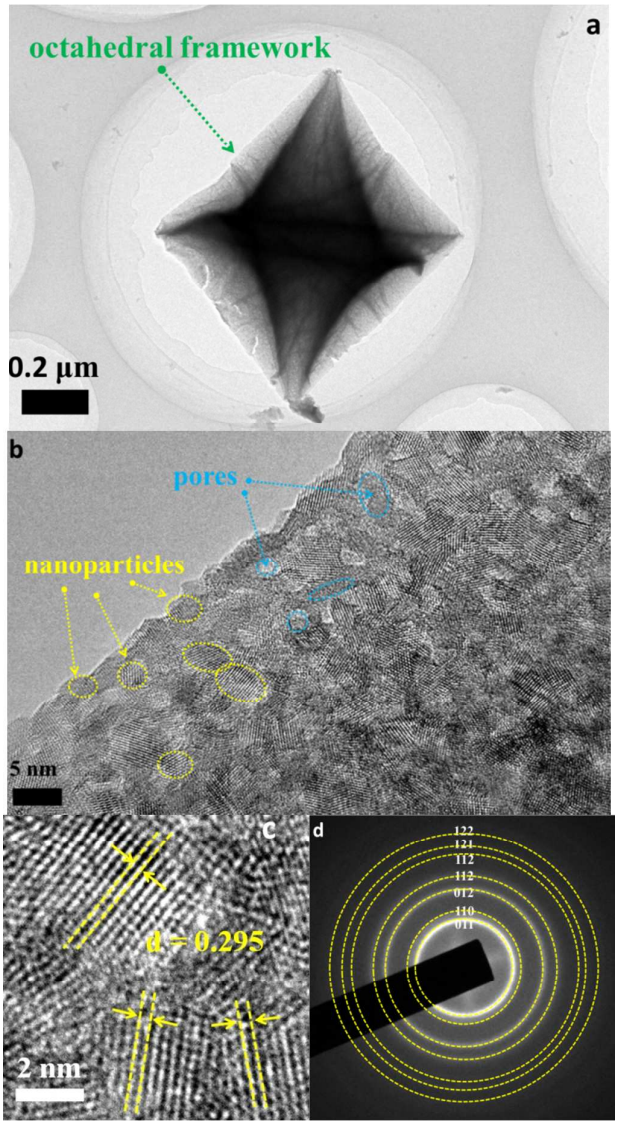

Fig. 4. (a, b) TEM images of t-ZrO_2, (c) high-resolution TEM image of representative zirconia nanoparticles, (d) SAED of t-ZrO_2.

A N_2 sorption analysis was carried out to evaluate the porous structure of the derived t-ZrO_2. Fig. 6 shows N_2 adsorption–desorption isotherm and pore size distribution of t-ZrO_2. The isotherm is of type IV based on IUPAC classification, characteristic for the formation of mesoporous materials.[22] The sample exhibits a hysteresis loop of Type E, which is typically featured as “ink-bottle” pores.[23] The main pore diameter value is 5–8 nm with a small portion of 3–4 nm. The

surface area is 174 m^2/g and the pore volume is 0.208 cm^3/g. The main reason for the development of porous t-ZrO_2 is attributed to the decomposition of the organic ligand in UiO-66. Furthermore, the broad temperature ranges for the removal of the organic species (Fig. S5) probably leads to the formation of broad pore size distribution.

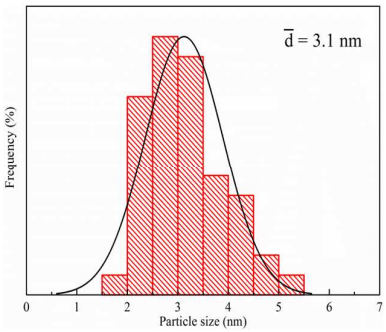

Fig. 5. Particle size distribution of t-ZrO_2.

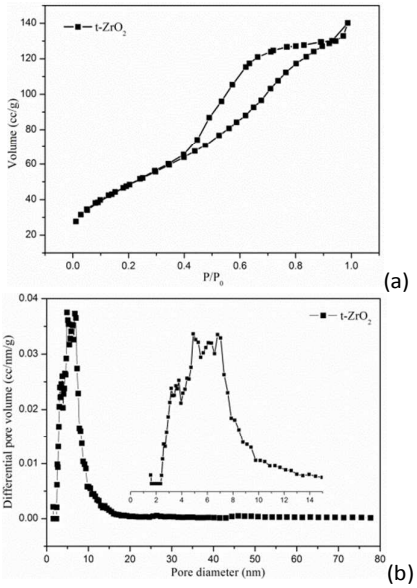

Fig. 6. (a) N_2 adsorption isotherm and (b) pore size distribution of t-ZrO_2.

Formation mechanism of mesoporous and octahedral t-ZrO_2 from thermal decomposition of UiO-66

Metal-organic frameworks (MOFs) have been successfully developed for the fabrication of nanoporous carbon materials.[24,25] By directly adjusting the carbonizing temperature of MOFs, the crystalline MOFs reorganized into aggregates of ultra-microporous carbon nanoparticles and retained their pristine morphology. These types of nanoporous carbon showed enhanced hydrogen storage capacity and excellent electrochemical properties. In our present work, special attention should be paid for the fabrication of metal oxides from the thermal decomposition of MOFs. A possible formation mechanism of octahedral t-ZrO_2 by thermal decomposition of UiO-66 is proposed and shown in Fig. 7. Thermal decomposition of UiO-66 causes the removal of 1, 4-benzenedicarboxylate ligands. With the escape of organic groups, the octahedral zirconia is reserved. The removal of the organic groups leads to the formation of mesoporous channels. Tetragonal zirconia, as one of the most desired structure, is vital for catalytic (superacid catalyst) and mechanical performances. However, it is difficult to stabilize the tetragonal phase at room temperature. Thus, great endeavors have been made to retain its tetragonal phase. The stabilization of the tetragonal phase can be accomplished by doping zirconia with suitable metal cations.[26–28] On the other hand, the stabilization of the tetragonal phase of zirconia mainly depends on its surface free energy. Only the high temperature polymorph has a lower surface free energy compared with the low temperature structure. The high temperature tetragonal phase of ZrO_2 could be stabilized at temperature below its normal transformation temperature.[29] The surface free energy of zirconia nanoparticles is greatly related with their crystallite size. If their size is below critical value, the surface energy of tetragonal phase is lower than that of monoclinic phase, which is favorable for the formation of t-ZrO_2.[29] In the present work, without the addition of stabilizers, t-ZrO_2 is synthesized by thermal decomposition from UiO-66 precursor. The stabilization of tetragonal of ZrO_2 is mainly attributed to the formation of small nanoparticles (3.1 nm).

In addition, the crystal-phase composition of ZrO_2 can also be controlled by nucleation kinetics in a non-aqueous benzyl alcohol route.[30] Reaction temperature played an important role on the formation of different phase of ZrO_2. At lower reaction temperature the monoclinic phase was formed predominantly, and almost pure phase of t-ZrO_2 was obtained at the highest temperature (270 °C). The reason for the result was ascribed to the formation of monoclinic embryos at lower temperature and a faster nucleation and growth of tetragonal phase at higher temperature. To verify the phase transformation, zirconia is synthesized by thermal decomposition of UiO-66 at 700 and 900 °C (Fig. S6). Apparently, the growth of monoclinic phase of ZrO_2 occurs at 700 °C, and is further enhanced at 900 °C. The result indicates the transformation of tetragonal to monoclinic phase of as-derived ZrO_2 with increasing reaction temperature. The result is consistent with the studies that tetragonal phase transformed into monoclinic phase at higher temperature in the synthesis of ZrO_2 by further thermal treatment, owing to the formation and growth of a monoclinic embryo during the thermal treatment.[30,31] Notably, as shown in Fig. 8, the octahedral morphology of as-derived zirconia is maintained at 700 and 900 °C. By comparing Fig. 2d, Fig. 8c and Fig. 8f, it is clear that the particle size of as-obtained zirconia grows larger with increasing reaction temperature and reaches ~60 nm at 900 °C. This suggests that the particle size of zirconia has a significant role on the composition.

The growth mechanism is similar to the escape-by-crafty-scheme strategy for the synthesis of metal oxide with inherited morphology from the transformation of crystalline coordination-polymer precursor.[32] The robust crystal structure

of the precursor and minimal structure reorganization during the transformation process mainly contributed to the maintained morphology and even the crystal plane orientation. On the basis of the above discussions, it can be concluded as following: (i) morphology-genetic material (UiO-66) used as a sacrifice template for the synthesis of ZrO_2 and the derived ZrO_2 inherited the octahedral structure; (ii) pure tetragonal ZrO_2 grew after thermal decomposition; (iii) mesoporous t-ZrO_2 with large surface area was produced; and (iv) t-ZrO_2 possessed small nanoparticles with the average particle size of 3.1 nm.

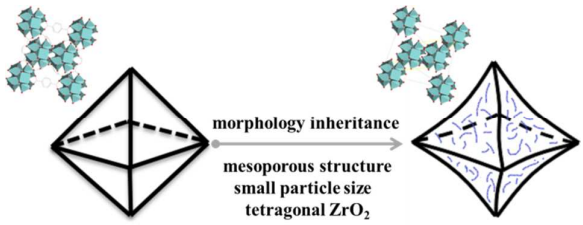

Fig. 7. Schematic of mechanism of formation of octahedral t-ZrO_2 from thermal decomposition of UiO-66.

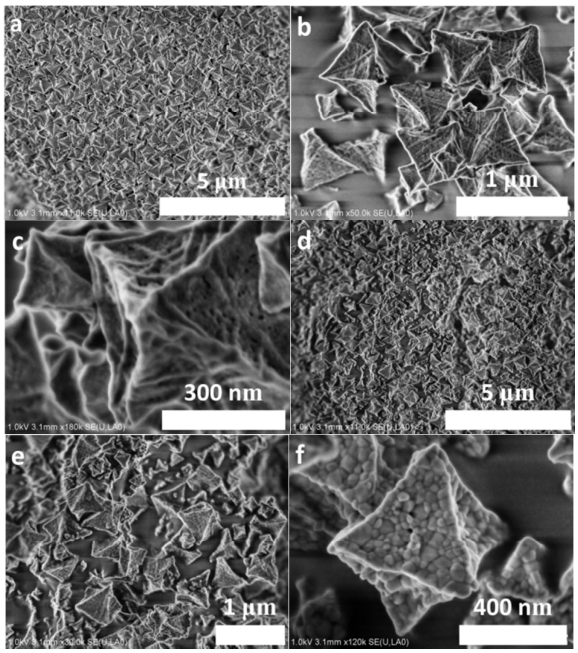

Fig. 8. SEM images of zirconia from thermal decomposition of UiO-66 at 700 °C (a, b, c) and 900 °C (d, e, f).

Application of MOFs-templated method to the fabrication of platelet t-ZrO_2

This growth methodology can also be used to design zirconia with platelet morphology through another type of UiO-66-HCl (Fig. 9). As shown in Fig. 9a and Fig. S7, XRD diffraction peaks of UiO-66-HCl disappear and the peaks for tetragonal phase of zirconia are observed. This suggests that the structure of the precursor is destroyed and pure t-ZrO_2-HCl is formed by thermal decomposition process. The overall morphology of as-obtained t-ZrO_2-HCl well maintains the platelet structure, which is inherited from the pristine precursor (Fig. 9b and Fig. S8). Fig. 9 c and d shows that zirconia presents the platelet morphology and small particle size with the lattice spacing of 0.295 nm corresponding to the (0 1 1) crystal face. The t-ZrO_2-HCl platelet exhibits mesoporous structure (Fig. 9e & f) and has the BET surface area of 147.3 m^2/g with the pore volume of 0.190 cm^3/g.

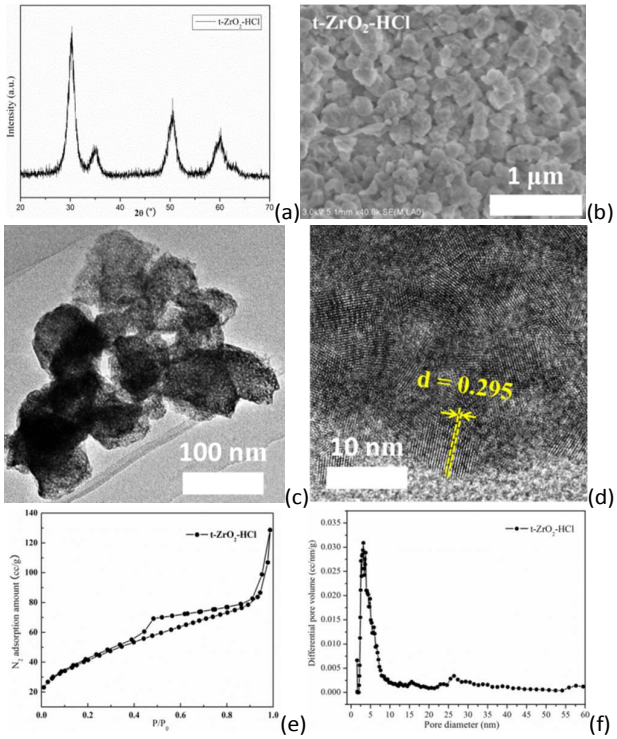

Fig. 9. (a) XRD pattern, (b) SEM image, (c, d) TEM images, N_2 adsorption isotherm (e), and pore size distribution (f) of t-ZrO_2-HCl.

Comparison of the methods for the fabrication of zirconia

The synthesis strategies for the porous zirconia have been summarized in Table 1, including hydrothermal, chemical vapor deposition (CVD), precipitation, and template method.[33–38] Based on the hydrothermal method, tetragonal or monoclinic zirconia with or without porous structure was produced. The further calcination was essential to transform the amorphous phase into tetragonal or monoclinic phase, but it easily caused the aggregation of the particles, which led to the decrease of the surface area.[34] ZrO_2/carbon aerogel was designed with the assistance of phenol formaldehyde resin in order to develop mesopore and tetragonal zirconia with a large surface area of 275.7 m^2 g^{-1}.[34] CVD method resulted in the formation of a mixture of the monoclinic and tetragonal phases.[35] For precipitation method, additional solvent or precipitating agent was required to fabricate t-ZrO_2. For example, zirconyl chloride octahydrate and ethylene diamine were used as zirconium precursor and precipitating agent, respectively, to produce ZrO_2 nanpartilces.[36] Factors of order of addition of the reactants, pH value, digestion time, digestion temperature, and digestion agents had significant effects on

the phase and particle size of ZrO_2. The phase composition depended on the experimental conditions during the preparation and the subsequent thermal treatment. Replica method by using hard template (SBA-15) was used to prepare ordered mesoporous ZrO_2, but the silicon could not be completely removed from the product.[37] Also, block copolymers as structure-directing agents allowed the formation of mesoporous t-ZrO_2 with large ordering lengths, thick semicrystalline walls, and large pores.[38] While it seems that the morphology-controllable synthesis of mesoporous t-ZrO_2 has not been well established. In this work, MOFs were explored to synthesize mesoporous t-ZrO_2 with predetermined morphology. MOFs performed as zirconium containing precursor and sacrifice template (for inherited morphology). The small particle size of zirconia was favorable to stabilize its tetragonal phase. Besides, the thermal calcination promoted the escape of organic groups, leading to the formation of mesoporous channels.

Conclusions

Controlled synthesis of porous t-ZrO_2 with desired morphology was realized from the thermal decomposition of metal-organic frameworks (UiO-66). This process avoids the use and removal of extra template as well as the addition of stabilizers for t-ZrO_2. The as-obtained zirconia showed pure tetragonal phase with small nanoparticles and mesoporous structure (large surface area 174 m^2/g). The proposed method for designing and synthesizing mesoporous t-ZrO_2 in this work is effective, simple and green. The morphological inheritance of t-ZrO_2 from UiO-66 gives new opportunities for fabrication of metal oxides with special structure using MOFs as templates. Furthermore, this method for the preparation of mesoporous zirconia can be used for other metal oxide mesoporous materials.

Acknowledgements

The financial supports from the National Natural Science Foundation of China (Nos. 21406153, 51451002, U1463209, 21376157) and Shanxi Province Science Foundation for Youths (No. 2014021014-2) are greatly appreciated. This work is also supported by Program for the Top Young Academic Leaders of Higher Learning Institutions of Shanxi Province.

Table 1. Comparison of experimental conditions and the results of previous studies with current work.

Oxide	Zr Precursor	Phase structure	Crystal size (nm)	Pore structure	Surface area (m^2/g)	Morphology	Method	Reaction temperature (°C)	References
ZrO_2	$Zr[(OCH_2)_3CH_3]_4$	tetragonal	7.52	none	184	microsphere	hydrothermal	200	33
ZrO_2	$ZrOCl_2{\cdot}8H_2O$	monoclinic	none	mesopore	23.7	nanoparticles	hydrothermal/calcination	180/800	34
ZrO_2/CA	$ZrOCl_2{\cdot}8H_2O$	tetragonal	none	mesopore	275.7	nanoparticles	hydrothermal/carbonization	180/800	34
ZrO_2	$Zr[OC(CH_3)_3]_4$	monoclinic/tetragonal	4.8/3.9	none	218	nanoparticles	CVD	500	35
ZrO_2	$ZrOCl_2{\cdot}8H_2O$	tetragonal	6.02/6.16	mesopore	193/157	nanoparticles	precipitation/calcination	800/900	36
ZrO_2	$ZrOCl_2{\cdot}8H_2O$	monoclinic/tetragonal	none	mesopore	220	rope	template	600	37
ZrO_2	$ZrCl_4$	tetragonal	2	mesopore	150	none	template	400	38
ZrO_2	UiO-66	tetragonal	3.1	mesopore	174	octahedron	template	500	this work
ZrO_2	UiO-66-HCl	tetragonal	4.5	mesopore	147.3	platelet	template	500	this work

Journal Name

ARTICLE

Notes and references

1 P. D. Yang, D. Y. Zhao, D. I. Margolese, B. F. Chmelka and G. D. Stucky, *Nature*, 1998, **396**, 152.
2 B. Kong, J. Tang, C. Selomulya, W. Li, J. Wei, Y. Fang, Y. C. Wang, G. F. Zheng and D. Y. Zhao, *J. Am. Chem. Soc.*, 2014, **136**, 6822.
3 S. Dutta and A. Bhaumik, *ChemSusChem*, 2013, **52**, 2039.
4 S.-H. Baeck, K.-S. Choi, T. F. Jaramillo, G. D. Stucky and E.W. McFarland, *Adv. Mater.*, 2003, **15**, 1269.
5 B. B. Wang, G. Wang and H. Wang, *Electrochim. Acta*, 2015, **156**, 1.
6 G. Z. Chen, F. Rosei and D. L. Ma, *Nanoscale*, 2015, **7**, 5578.
7 S. R. Deng, M. Kurttepeli, D. J. Cott, S. Balsb and C. Detavernier, *J. Mater. Chem. A*, 2015, **3**, 2642.
8 Q. T. Guo, P. With, Y. Liu, R. Gläser and C.-J. Liu, *Catal. Today*, 2013, **211**, 156.
9 P. P. Su, S. C. Liao, F. Rong, F. Q. Wang, J. Chen, C. Li and Q. H. Yang, *J. Mater. Chem. A*, 2014, **2**, 17408.
10 W. Cho, S. Park and M. Oh, *Chem. Commun.*, 2011, **47**, 4138.
11 V. P. Santos, T. A. Wezendonk, J. J. D. Jaén, A. I. Dugulan, M. A. Nasalevich, H.-U. Islam, A. Chojecki, S. Sartipi, X. H. Sun, A. A. Hakeem, A. C. J. Koeken, M. Ruitenbeek, T. Davidian, G. R. Meima, G. Sankar, F. Kapteijn, M. Makkee and J. Gascon, *Nat. Commun.*, 2015, **6**, 6451.
12 H. H. Zhao, H. L. Song, L. L. Xu and L. J. Chou, *Appl. Catal. A*, 2013, **456**, 188.
13 J.-K. Sun and Q. Xu, *Energy Environ. Sci.*, 2014, **7**, 2071.
14 Y. H. Song, X. Li, L. L. Sun and L. Wang, *RSC Adv.*, 2015, **5**, 7267.
15 Z. F. Yue, S. C. Liu and Y. Liu, *RSC Adv.*, 2015, **5**, 10619
16 A. A. Voskanyan, C.-Y. V. Li, K.-Y. Chan and L. Gao, *CrystEngComm*, 2015, **17**, 2620.
17 G. Lu, C. L. Cui, W. N. Zhang, Y. Y. Liu and F. W. Huo, *Chem. Asian J.*, 2013, **8**, 69.
18 P. S. Bárcia, D. Guimarães, P. A. P. Mendes, J. A. C. Silva, V. Guillerm, H. Chevreau, C. Serre and A. E. Rodrigues, *Micropor. Mesopor. Mater.*, 2011, **139**, 67.
19 Y. Liu and H.-X. He, *Micropor. Mesopor. Mater.*, 2013, **165**, 27.
20 D. D. Liu, F. N. Dai, H. Liu, Y. Q. Liu and C. G. Liu, *Mater. Lett.*, 2015, **139**, 7.
21 F. Davar, A. Hassankhani and M. R. Loghman-Estarki, *Ceram. Int.*, 2013, **39**, 2933.
22 K. S. W. Sing, D. H. Everett, R. A. W. Haul, L. Moscou, R. A. Pierotti, J. Rouquérol and T. Siemieniewska, *Pure Appl. Chem.*, 1985, **57**, 603.
23 J. H. De Boer, B. C. Lippens, B. G. Linsen, J. C. P. Broekhoff, A. van den Heuvel and Th. J. Osinga, *J. Colloid Interface Sci.*, 1958, **21**, 405.
24 B. Liu, H. Shioyama, H. L. Jiang, X. B. Zhang and Q. Xu, *Carbon*, 2010, **48**, 456.
25 S. J. Yang, T. Kim, J. H. Im, Y. S. Kim, K. Lee, H. Jung and C. R. Park, *Chem. Mater.*, 2012, **24**, 464.
26 C. F. Grain, *J. Am. Ceram. Soc.*, 1967, **50**, 288.
27 M. R. Loghman-Estarki, M. Nejati, H. Edris, R. S. Razavi, H. Jamali and A. H. Pakseresht, *J. Eur. Ceram. Soc.*, 2015, **35**, 693.
28 M. R. Loghman-Estarki, M. Hajizadeh-Oghaz, H. Edris and R. S. Razavi, *CrystEngComm,* 2013, **15**, 5898.
29 R. C. Garvie and M. F. Goss, *J. Mater. Sci.*, 1986, **21**, 1253.
30 T. A. Cheema and G, Garnweitner, *CrystEngComm*, 2014, **16**, 3366.
31 D. A. Ward and E. I. KO, *Chem. Mater.*, 1993, **5**, 956.
32 J. Zhao, M. R. Li, J. L. Sun, L. F. Liu, P. P. Su, Q. H. Yang and C. Li, *Chem. Eur. J.*, 2012, **18**, 3163.
33 D. S. S. Padovini, D. S. L. Pontes, C. J. Dalmaschio, F. M. Pontes and E. Longo, *RSC Adv.*, 2014, **4**, 38484.
34 Y.-F. Lin and F.-L. Liang, *CrystEngComm,* 2015, **17**, 678.
35 S. Benfer and E. Knözinger, *J. Mater. Chem.*, 1999, **9**, 1203.
36 V. G. Deshmane and Y. G. Adewuyi, *Micropor. Mesopor. Mater.*, 2012, **148**, 88.
37 B. Liu and R. T. Baker, *J. Mater. Chem.*, 2008, **18**, 5200.
38 P. D. Yang, D. Y. Zhao, D. I. Margolese, B. F. Chmelka and G. D. Stucky, *Chem. Mater.*, 1999, **11**, 2813.

Synthesis of mesporous and tetragonal zirconia with inherited morphology from metal-organic frameworks

Xiaoliang Yan, Ningyue Lu, Binbin Fan*, Jiehua Bao, Dahai Pan, Meijun Wang and Ruifeng Li*

College of Chemistry and Chemical Engineering, Taiyuan University of Technology, Taiyuan 030024, China

*Corresponding author. Tel.: +86 351 6018384; Fax: +86 351 6010121.

E-mail: yanxiaoliang@tyut.edu.cn, fanbinbin@tyut.edu.cn, rfli@tyut.edu.cn

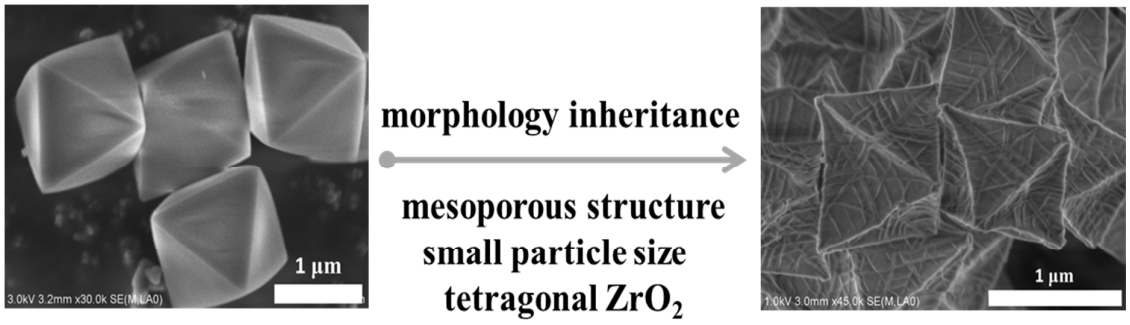

Controlled synthesis of porous and tetragonal zirconia with octahedral morphology was proposed from the thermal decomposition of UiO-66.